Restricted diffusion and the return to the origin probability at intermediate and long times

Lawrence M. Schwartz and Martin D. Hürlimann
Schlumberger-Doll Research, Old Quarry Road, Ridgefield, Connecticut 06877-4108

Keh-Jim Dunn
Chevron Petroleum Technology Company, P.O. Box 446, La Habra, California 90633-0446

Partha P. Mitra
AT&T Bell Laboratories, Murray Hill, New Jersey 07974

David J. Bergman
School of Physics and Astronomy, Raymond and Beverly Sackler Faculty of Exact Sciences, Tel Aviv University, Tel Aviv 69978, Israel
(Received 3 June 1996)

Pulsed field gradient spin echo magnetic resonance measurements on fluid saturated porous media provide a natural framework for the examination of a classic problem in mathematical physics. We examine the overall time dependence of the return to the origin probability (RTOP) with particular emphasis on the intermediate and long time behavior. In the long time limit this probability is related to the electrical conductivity. In periodic geometries we compare the results of eigenvalue expansions and numerical simulations. Here we find that, when the diffusion length is roughly equal to a pore diameter, the normalized RTOP, $P_s(t)$, shows a maximum. Thus, the approach to the long time limit is *not* monotonic. We show that the existence of this maximum can be predicted based on variational arguments. For disordered systems, simulations and experiments are found to be in agreement and again suggest that the behavoir of $P_s(t)$ is not monotonic. [S1063-651X(97)06304-6]

PACS number(s): 05.60.+w, 66.10.Cb

I. INTRODUCTION

Transport and diffusion in three-dimensional porous media are important in connection with problems relating to a wide range of materials, e.g., reservoir rocks, catalytic beds, foams, and ceramic composites. In an important subset of these problems one is concerned with systems comprised of an insulating, solid granular matrix saturated with a conducting pore fluid. Within this framework, the transport problem is closely related to the inverse problem studied by Kac in a classic paper entitled ''Can one hear the shape of a drum?'' [1]. (de Gennes [2] has studied a related problem in the context of magnetization decay in a bounded region.) Briefly, the question is whether or not the structure (i.e., shape) of the boundary can be determined from a knowledge of the diffusion equation's eigenvalue spectrum [3–5].

An important aspect of restricted diffusion is the choice of boundary condition at the pore-matrix interface. However, the issues of interest in this paper are easily understood even with the simple assumption that the boundaries are perfectly reflecting (i.e., that interfacial absorbtion can be neglected). Making this assumption, we consider two of the time (t) dependent quantities studied by Kac [1], the diffusion coefficient, $D(t)\equiv\langle|\mathbf{r}(t)|^2\rangle/(6t)$, and the spectral function, $P(t)\equiv(1/V_p)\Sigma_\lambda e^{-\lambda t}$. Here $\mathbf{r}(t)$ denotes the position of a diffusing particle and $\{\lambda\}$ are the eigenvalues of the equations describing diffusion in the pore space of volume V_p. We will see that $P(t)$ is related to the probability that a diffusing particle returns to its point of origin at time t. By convention, both $D(t)$ and $P(t)$ are usually normalized with respect to their values for unrestricted diffusion. For $D(t)$ this amounts to simply dividing by D_0, the diffusion constant for the bulk fluid. Similarly, for $P(t)$ we divide by $P_0(t)=(4\pi D_0 t)^{-3/2}$ to obtain the normalized return to the origin probability

$$P_s(t)\equiv\frac{(4\pi D_0 t)^{3/2}}{V_p}\sum_\lambda e^{-\lambda t}. \tag{1.1}$$

Interestingly, $D(t)$ and $P_s(t)$ have in common the fact that, as $t\to 0$, the variation of both functions is determined by a length scale of physical interest, V_p/S, the ratio of the pore space volume to its surface area [6–9]:

$$D(t)/D_0=1-\frac{4S}{9\sqrt{\pi}V_p}\sqrt{D_0 t}+O(D_0 t), \tag{1.2}$$

$$P_s(t)=1+\frac{\sqrt{\pi}}{2}\frac{S}{V_p}\sqrt{D_0 t}+O(D_0 t). \tag{1.3}$$

Physically, the signs of these corrections are easily understood: diffusive motion in the pore space is hindered by the solid matrix, *reducing* the mean square distance traveled by the particles while *increasing* the return to the origin probability (RTOP).

At long times, both $D(t)$ and $P_s(t)$ tend to limiting values that depend only on the lowest lying eigenvalues. However, at intermediate times they both depend on the entire spectrum of eigenvalues, albeit in somewhat different ways. A number of theoretical and experimental studies have shown that $D(t)$ decreases monotonically from the value D_0 to the

long time limit D_{eff}, which can be determined, independently, from the dc electrical conductivity, σ_{eff} [10,11]. Very little, however, is known about the overall time dependence of $P_s(t)$, except that, in periodic systems without any interfacial relaxation, this quantity has been shown to approach the long time asymptote $\phi^{-1}(D_0/D_{\text{eff}})^{3/2}$ [8]. (Here the porosity ϕ denotes the volume fraction assigned to the pore space.) Accordingly, we have undertaken a detailed study of this quantity and have found that $P_s(t)$ exhibits considerably more varied and interesting behavior than $D(t)$. For this reason we believe that $P_s(t)$ will be an important indicator of the structure of the underlying porous media. Our findings are as follows:

(a) In periodic porous media $P_s(t)$ can be calculated by either eigenvalue expansions or by numerical simulations. In the absence of interfacial relaxation, both techniques predict that $P_s(t)$ crosses above its long time asymptote and exhibits a well defined *maximum* at intermediate times. This is enhanced by either interfacial relaxation or grain consolidation to lower porosities.

(b) This behavior is predicted by a new theorem that constrains the shape of the lowest eigenvalue band. Additional developments in this direction are discussed by Bergman [12].

(c) In disordered bead packs numerical simulations predict nonmonotonic behavior for $P_s(t)$. As in the ordered case, this effect becomes more pronounced as the bead pack is consolidated at lower porosities. Experimental results on unconsolidated bead packs are in reasonable agreement with the simulations, again suggesting nonmonotonic behavior for $P_s(t)$.

(d) Systematic trends appear to relate the way that $P_s(t)$ moves away from its short time behavior (1.3) to the tortuosity of the pore space.

II. PGSE MEASUREMENTS AND THE RETURN TO THE ORIGIN PROBABILITY

Pulsed field gradient spin echo (PGSE) nuclear magnetic resonance (NMR) measurements provide an important probe of the restricted diffusive motion of water molecules through porous media and biological tissue [13–16]. There have been a number of recent investigations regarding the relationship between the microgeometry that restricts the motion of water molecules and the PGSE amplitude [17–24]. In a PGSE experiment, the spin echo radio frequency pulse sequence is combined with the application of two gradient pulses, separated by a time t, each of which briefly imposes a spatial dependence on the static magnetic field. In the limit that the duration δ of each gradient pulse approaches zero as its amplitude g approaches infinity (such that δg remains finite) the interpretation of this measurement simplifies considerably. Physically, the two gradient pulses can then be viewed as instantaneously dephasing and then rephasing the spins involved in the underlying spin echo measurement. In the absence of diffusion, these two effects cancel exactly. However, if a spin originally at $\mathbf{r}$ diffuses to $\mathbf{r}'$ at time t, when the second gradient pulse is applied, its net phase change is $\mathbf{k}\cdot(\mathbf{r}-\mathbf{r}')$, where $\mathbf{k}=\gamma\delta\mathbf{g}$, γ is the gyromagnetic ratio, and $\mathbf{g}$ is a vector along the gradient direction with magnitude g. In this case, the decay of the echo amplitude is directly related to the problem of self-diffusion in restricted geometries. In practice, however, PGSE measurements in porous media are complicated by the fact that the gradient pulses are never infinitely sharp so that diffusion *during* the pulse application must be taken into account. The implications of this effect will be discussed in Sec. III C; the following development will assume that ideal conditions are obtained so that the PGSE amplitude, $M(\mathbf{k},t)$, can be expressed in terms of the Fourier transform of the diffusion propagator, $G(\mathbf{r},\mathbf{r}_1,t)$.

A. General equations

Given the molecular diffusion coefficient D_0 of the bulk fluid, the propagator $G(\mathbf{r},\mathbf{r}_1,t)$, for $\mathbf{r}$ and $\mathbf{r}_1$ in the pore space, is defined by the equations

$$\frac{\partial G(\mathbf{r},\mathbf{r}_1,t)}{\partial t}=D_0\nabla^2 G(\mathbf{r},\mathbf{r}_1,t), \tag{2.1}$$

$$G(\mathbf{r},\mathbf{r}_1,t=0^+)=\delta^3(\mathbf{r}-\mathbf{r}_1), \tag{2.2}$$

$$D_0\hat{\mathbf{n}}\{\nabla G(\mathbf{r},\mathbf{r}_1,t)+\rho G(\mathbf{r},\mathbf{r}_1,t)\}_{\mathbf{r}\in\Sigma}=0, \tag{2.3}$$

where $\hat{\mathbf{n}}$ is the outward (from pore to grain) directed normal unit vector at the pore-grain interface Σ, and the parameter ρ determines the strength of the enhanced interfacial spin relaxation. Under the assumptions outlined above, the PGSE amplitude $M(\mathbf{k},t)$ is given by the double spatial Fourier transform

$$M(\mathbf{k},t)=\frac{1}{V_p}\int_{V_p}d\mathbf{r}\int_{V_p}d\mathbf{r}_1 G(\mathbf{r},\mathbf{r}_1,t)e^{-i\mathbf{k}\cdot(\mathbf{r}-\mathbf{r}_1)}, \tag{2.4}$$

where V_p is the total volume of the pore space. The quantity $M(t)\equiv M(\mathbf{k}=\mathbf{0},t)$ represents the total magnetization of the system. For $\rho=0$ it has the constant value 1, but for $\rho>0$ it decays in time from $M(0)=1$ to $M(\infty)=0$. For small $\mathbf{k}$, $M(\mathbf{k},t)$ has the simple form [6,7]

$$\frac{M(\mathbf{k},t)}{M(t)}=e^{-D(t)k^2t}. \tag{2.5}$$

This relation defines the effective time dependent diffusion coefficient $D(t)$, which characterizes the long wavelength behavior of the PGSE amplitude. In the limit $\rho\to 0$, $D_{\text{eff}}\equiv D(t\to\infty)$ is directly related to the electrical conductivity of the fluid saturated porous medium and can be determined experimentally by routine measurements [11]. The time dependent diffusion coefficient $D(t)$ can be calculated either from values of $M(\mathbf{k},t)$ at small $\mathbf{k}$ vectors or from the mean square displacement of a diffusing particle, $\langle[\mathbf{r}(t)]^2\rangle=6D(t)t$.

In principle, by integrating Eq. (2.4) over all of $\mathbf{k}$ space, we obtain

$$P(t|\rho)\equiv\int M(\mathbf{k},t)\frac{d\mathbf{k}}{(2\pi)^3}=\frac{1}{V_p}\int_{V_p}G(\mathbf{r},\mathbf{r},t)d\mathbf{r}. \tag{2.6}$$

By definition, this is the RTOP density averaged over all possible initial positions of the diffusing particle. Clearly, this quantity carries information about the degree of restrictions to diffusion in a porous medium. Equation (2.6) also provides a way of obtaining the RTOP from PGSE data. In free space the time dependence of $P(t|\rho)$ can be evaluated analytically, $P(t|\rho)\rightarrow P_0(t)=(4\pi D_0 t)^{-3/2}$. As long as we are dealing with a percolating (interconnected) pore space, it is clear that the RTOP must decay to zero at long times. If we also have $\rho\neq 0$, then part of the enhanced decay with time of $P(t|\rho)$ is due to the decay of the total spin polarization, which is described by $M(t)$. Therefore, in order to isolate the effects of the interface on the RTOP, we normalize $P(t|\rho)$ with respect to both $P_0(t)$ and $M(t)$:

$$P_s(t|\rho)\equiv\frac{P(t|\rho)}{M(t)P_0(t)}. \tag{2.7}$$

In order to make contact with the discussion in the Introduction, we note that

$$\lim_{\rho\rightarrow 0}P(t|\rho)=P(t), \tag{2.8}$$

$$\lim_{\rho\rightarrow 0}P_s(t|\rho)=P_s(t). \tag{2.9}$$

B. Results for periodic systems

The diffusion propagator can always be expanded in terms of a set of orthonormal diffusion eigenstates [22,24]. When the microstructure is periodic, the eigenfunctions have the Bloch-Floquet form, $u_{n\mathbf{q}}(\mathbf{r})e^{i\mathbf{q}\cdot\mathbf{r}-\lambda_{n\mathbf{q}}t}$, where $\lambda_{n\mathbf{q}}$ is the eigenvalue, n is a band index, $\mathbf{q}$ is a wave vector in the first Brillouin zone of reciprocal space, and the periodic function, $u_{n\mathbf{q}}(\mathbf{r})$, satisfies the following equations:

$$\lambda_{n\mathbf{q}}u_{n\mathbf{q}}(\mathbf{r})+D_0(\nabla+i\mathbf{q})^2u_{n\mathbf{q}}(\mathbf{r})=0, \tag{2.10}$$

$$\{D_0\hat{\mathbf{n}}\cdot(\nabla+i\mathbf{q})u_{n\mathbf{q}}(\mathbf{r})+\rho u_{n\mathbf{q}}(\mathbf{r})\}_{\mathbf{r}\in\Sigma}=0, \tag{2.11}$$

$$\int_{V_p}dV u^*_{n\mathbf{q}}(\mathbf{r})u_{m\mathbf{q}}(\mathbf{r})=\delta_{nm}. \tag{2.12}$$

The function $u_{n\mathbf{q}}(\mathbf{r})$, restricted to the pore space V_p, can be expanded in a Fourier series

$$\theta_p(\mathbf{r})u_{n\mathbf{q}}(\mathbf{r})=\sum_{\mathbf{G}}\tilde{u}_{n\mathbf{q}}(\mathbf{G})e^{i\mathbf{G}\cdot\mathbf{r}}, \tag{2.13}$$

where $\theta_p(\mathbf{r})$ is the characteristic (or indicator) function of the pore space, equal to 1 inside that pore space and to 0 elsewhere. The diffusion propagator can now be written as

$$G(\mathbf{r},\mathbf{r}',t)=\sum_{n\mathbf{q}}e^{-\lambda_{n\mathbf{q}}t}u_{n\mathbf{q}}(\mathbf{r})u^*_{n\mathbf{q}}(\mathbf{r}')e^{i\mathbf{q}\cdot(\mathbf{r}-\mathbf{r}')}. \tag{2.14}$$

The PGSE amplitude has a particularly concise expression in terms of the Fourier expansion coefficients $\tilde{u}_{n\mathbf{q}}(\mathbf{G})$

$$M(\mathbf{k},t)=\frac{V_p}{\phi^2}\sum_n e^{-\lambda_{n\mathbf{q}}t}[|\tilde{u}_{n\mathbf{q}}(\mathbf{G}_\mathbf{k})|^2]_{\mathbf{q}=\mathbf{k}-\mathbf{G}_\mathbf{k}}, \tag{2.15}$$

where $\phi\equiv V_p/V$ is the porosity and $\mathbf{G}_\mathbf{k}$ is the reciprocal lattice vector that is closest to $\mathbf{k}$. For small $\mathbf{k}$, we have $\mathbf{G}_\mathbf{k}=\mathbf{0}$ and $\mathbf{q}=\mathbf{k}$.

To evaluate the RTOP, we note that within the present framework Eq. (2.7) reduces to

$$P_s(t|\rho)=\frac{(4\pi D_0 t)^{3/2}}{V_pM(t)}\sum_{n\mathbf{q}}e^{-\lambda_{n\mathbf{q}}t}, \tag{2.16}$$

where

$$M(t)=\frac{V_p}{\phi^2}\sum_n e^{-\lambda_{n\mathbf{0}}t}|\tilde{u}_{n\mathbf{0}}(\mathbf{0})|^2. \tag{2.17}$$

From the above analysis it is clear that, in periodic systems, the RTOP carries information about the connectivity of the pore space. At long times, both $P_s(t)$ and $M(t)$ depend only on the lowest lying eigenstates. In the case of $M(t)$ this means the state $u_{0\mathbf{0}}$, while in the case of $P_s(t)$ this means the small $\mathbf{q}$ states of the lowest band $u_{0\mathbf{q}}$. In the case of a porous medium with cubic symmetry, these low lying eigenvalues have the form

$$\lambda_{0\mathbf{q}}=\lambda_{0\mathbf{0}}(\rho)+D_{\mathrm{eff}}(\rho)q^2+O(q^4), \tag{2.18}$$

where $\lambda_{0\mathbf{0}}=0$ if $\rho=0$. [The qualitative dependence of $D_{\mathrm{eff}}(\rho)$ on ρ is discussed in Refs. [11] and [24].] Thus, for a periodic cubic porous medium, the sums over n in both Eqs. (2.16) and (2.17) reduce to the single term $n=0$, while the sum over $\mathbf{q}$ in Eq. (2.16) becomes a Gaussian integral, with a result that partially cancels the prefactor $(4\pi D_0 t)^{3/2}$. The remaining exponential time dependence $e^{-\lambda_{0\mathbf{0}}t}$ also cancels, and we get

$$\lim_{t\rightarrow\infty}P_s(t|\rho)=\frac{V}{|\int_{V_p}dV u_{0\mathbf{0}}(\mathbf{r})|^2}\left(\frac{D_0}{D_{\mathrm{eff}}(\rho)}\right)^{3/2} \tag{2.19}$$

$$\geqslant\frac{1}{\phi}\left(\frac{D_0}{D_{\mathrm{eff}}(\rho)}\right)^{3/2}, \tag{2.20}$$

where we used the Cauchy-Schwartz inequality, along with Eq. (2.12), to get an upper bound on the integral

$$\left|\int_{V_p}dV u_{0\mathbf{0}}(\mathbf{r})\right|^2\leqslant\int_{V_p}dV|u_{0\mathbf{0}}|^2\int_{V_p}dV=V_p. \tag{2.21}$$

For $\rho=0$, $u_{0\mathbf{0}}(\mathbf{r})=1/\sqrt{V_p}=\mathrm{const}$ [23], and the inequality sign in these equations becomes an equality. The right-hand side (rhs) of Eq. (2.19) was first proposed as the limiting form for $P_s(t)$ at long times based on a phenomenological ansatz [6], which assumed that the PGSE amplitude is given, approximately, by the convolution of an effective Gaussian

and the pore space two point correlation function [6,7]. Here we have *proved* this result for the quantity

$$P_s(t) \equiv \lim_{\rho \to 0} P_s(t|\rho) \tag{2.22}$$

for any periodic cubic porous medium. Otherwise, when $\rho \neq 0$, the rhs of Eq. (2.19) is only a lower bound for the asymptote of $P_s(t)$. In fact, the results of Eqs. (2.19) and (2.20) can be extended to more general (i.e., anisotropic) periodic structures, and to certain nonperiodic structures as well [12].

Most of the results presented in this paper will concern the limiting case of Eq. (2.22). Here we can make a precise statement about the way $P_s(t)$ approaches its long time asymptote. Following the same idea that led to Eq. (2.19), we can write the following expression for the long time behavior of $P_s(t)$ for that case:

$$P_s(t) \cong \frac{(4\pi D_0 t)^{3/2}}{\phi} \int \frac{d^3q}{(2\pi)^3} e^{-\lambda_{0\mathbf{q}} t}. \tag{2.23}$$

We now show that, not only is $\lambda_{0\mathbf{q}}$ well approximated by the parabola $D_{\text{eff}} q^2$ for small $\mathbf{q}$, but that $\lambda_{0\mathbf{q}}$ lies below that parabola for *arbitrary* $\mathbf{q}$. Due to the variational properties of the diffusion problem, $\lambda_{0\mathbf{q}}$ can be obtained as the minimum value of the following integral [12]:

$$D_0 \int_{V_p} dV |\nabla \psi|^2, \tag{2.24}$$

where $\psi(\mathbf{r})$ is an arbitrary normalized Bloch function, i.e.,

$$\int_{V_p} dV |\psi|^2 = 1, \tag{2.25}$$

$$\psi(\mathbf{r}+\mathbf{a}) = e^{i\mathbf{q}\cdot\mathbf{a}} \psi(\mathbf{r}) \tag{2.26}$$

for any lattice vector $\mathbf{a}$. We can therefore get an upper bound on $\lambda_{0\mathbf{q}}$ by using the following trial function in Eq. (2.24):

$$\psi(\mathbf{r}) = \frac{e^{i\mathbf{q}\cdot\mathbf{f}(\mathbf{r})}}{\sqrt{V_p}}, \tag{2.27}$$

where $f_\alpha(\mathbf{r})$ is the solution of a stationary diffusion problem in the same porous medium

$$\nabla^2 f_\alpha(\mathbf{r}) = 0 \text{ in } V_p, \tag{2.28}$$

$$\frac{\partial f_\alpha}{\partial n} = 0 \text{ at the interface}, \tag{2.29}$$

$$f_\alpha(\mathbf{r}) - r_\alpha \text{ is a periodic function}. \tag{2.30}$$

In this way we get, for a system with a periodic cubic microstructure,

$$\lambda_{0\mathbf{q}} < D_0 \frac{1}{V_p} \int_{V_p} dV |\nabla(\mathbf{q}\cdot\mathbf{f})|^2 = D_{\text{eff}}\, q^2. \tag{2.31}$$

The last equality is related to the connection, alluded to previously, between D_{eff} and the bulk effective conductivity σ_{eff} of the same porous medium, where the grains are insulating and the pore space has a nonzero conductivity σ_0 [23]:

$$\frac{D_{\text{eff}}}{D_0} = \frac{1}{\phi} \frac{\sigma_{\text{eff}}}{\sigma_0} = \frac{1}{\phi F}. \tag{2.32}$$

Here F is the so-called ''formation factor'' of the porous medium. Thus, (2.28)–(2.30) can be reinterpreted as equations for the electric potential in such a system. In that case, it is well known that, for an electrically isotropic metal-insulator composite, we have [25,26]

$$\frac{\sigma_{\text{eff}}}{\sigma_0} \delta_{\alpha\beta} = \frac{1}{V} \int_{V_p} dV (\nabla f_\alpha \cdot \nabla f_\beta). \tag{2.33}$$

From Eq. (2.31) it follows that, for sufficiently long times, we can write

$$P_s(t) > \frac{(4\pi D_0 t)^{3/2}}{\phi} \int \frac{d^3q}{(2\pi)^3} e^{-D_{\text{eff}} q^2 t} = \frac{1}{\phi} \left(\frac{D_0}{D_{\text{eff}}} \right)^{3/2}. \tag{2.34}$$

Thus, $P_s(t)$ approaches its $t = \infty$ value from above, and consequently it *must* have a maximum at some intermediate time.

These results actually have a very general validity: they can be extended to the case of nonzero surface relaxation $\rho \neq 0$, to an anisotropic medium, and to a nonperiodic porous medium [12].

III. COMPUTATIONAL AND EXPERIMENTAL TECHNIQUES

A. Random walker simulations

Given a direct representation of the pore geometry, the PGSE amplitude can be calculated by random walk simulations of diffusing particles [9,27,28]. In the present paper we will be concerned with two systems, both of which are based on the packing of spherical grains. The first is an ordered structure in which identical grains are arranged on a simple cubic lattice; the second is a disordered three-dimensional packing of nearly monosized spherical grains. The second system is comprised of a $20 \times 20 \times 40$ dense random packing with periodic boundary conditions in the x and y directions [9,27,28]. Because this packing is *not* periodic in the z direction, random walkers are only released within a band centered at the system's midheight. The packing is large enough in the z direction that, in the time scales of interest here, walkers never diffuse to reach the system's top or bottom. This packing is large enough to provide a reasonable average over the different configurations found in disordered sphere packs. The grain radii for the dense random packing vary by $\pm 8\%$ to reflect the experimental variations present in nominally *monosized* packings. The porosity of both systems can be varied by application of the grain consolidation algorithm [29]; the centers of the grains remain fixed while the sphere radius is increased.

In the present simulations random walkers move through the pore space taking steps of fixed length ϵ, with the clock

advancing by $\tau=\epsilon^2/(6D_0)$ at each step. Since we are primarily interested in the behavior of long time diffusion, relatively large step sizes were employed. For the cubic packing ϵ was taken to be equal to $0.01a$, where a is the (fixed) edge length of the unit cell. In the dense random packing, $\epsilon=0.02R_0$, where R_0 is the midpoint of the original distribution of sphere radii. (When the packings are unconsolidated, $a/2$ is the radius of the spheres on the cubic lattice, so the two values of ϵ are roughly comparable.) Walkers are launched from randomly chosen positions (x_0,y_0,z_0) within the pore space and, at each time step of size τ, advance from their current position (x_1,y_1,z_1) to a new position (x_2,y_2,z_2) on the surface of a sphere of radius ϵ. Implementation of the boundary condition (2.3) is, in principle, straightforward [28] as long as the absorption strength ρ is reasonably weak (as is the case in almost all experiments of interest). In fact, all of the simulation results to be discussed in this paper are confined to the case $\rho=0$. In this limit we have *blind* reflection at the pore-grain interface; the walker returns to its attempt position and the clock advances by one time step τ. Because it is well known that long time diffusion behavior is difficult to simulate, and because a nonzero value of ρ exacerbates that situation [11], we have chosen to focus here on the $\rho\rightarrow 0$ limit. Even with this assumption, we will see that the statistical uncertainties involved in the calculation of $P_s(t)$ are quite formidable. To evaluate the RTOP, at a prespecified array of times $\{t_n\}$ we calculate the number of walkers whose distance from their starting point lies between $R_{m-1}\equiv(m-1)\,\delta R$ and $R_m\equiv m\,\delta R$. The bin size δR must be comparable to (but not commensurate with) the random walk step size; in the present simulations we take $\delta R/a$ [or $\delta R/(2R_0)$] equal to $\pi/400$. Thus the simulations provide a discrete representation of the probability, $P(R_m,t_n)$, that walkers will be located in the mth spatial bin after time t_n. In practice, of course, a given walker will never return *exactly* to its point of origin. Accordingly, we are led to consider the quantity

$$P(\Delta R,t)=\frac{1}{V_p}\int_{V_p}d\mathbf{r}_1\int_{|\mathbf{r}|\leq\Delta R}d\mathbf{r}G(\mathbf{r}_1,\mathbf{r}+\mathbf{r}_1,t). \quad (3.1)$$

$P(\Delta R,t)$ is by definition the probability that a diffusing particle will return to within ΔR of its starting point after time t, averaged over all possible initial positions [8,9]. (In practice, the values of ΔR employed in our simulations were multiples of $4\delta R$, so that the inequality $\Delta R>\epsilon$ was always satisfied.) For the case of diffusion in a homogeneous fluid,

$$P(\Delta R,t)\rightarrow P_0(\Delta R,t)=\frac{4\pi(\Delta R)^3}{3(4\pi D_0 t)^{3/2}}, \quad (3.2)$$

as long as $(\Delta R)^2\ll 4D_0t$. By analogy with Eq. (2.7), we introduce the normalized quantity $P_s(\Delta R,t)$:

$$P_s(\Delta R,t)=\frac{P(\Delta R,t)}{P_0(\Delta R,t)}. \quad (3.3)$$

To leading order in ΔR, one has the expansion [21,9]

$$P_s(\Delta R,t)=P_s(\Delta R=0,t)\left[1-\frac{3\Gamma(t)}{16}\frac{S}{V_p}\Delta R+O((\Delta R)^2)\right]. \quad (3.4)$$

where

$$\Gamma(t)\equiv\frac{\langle G(\mathbf{r},\mathbf{r},t)\rangle_\Sigma}{\langle G(\mathbf{r},\mathbf{r},t)\rangle_{V_p}}. \quad (3.5)$$

$\Gamma(t)$ is the ratio of the RTOP for particles originating on the interface to that for particles originating in the bulk. $\Gamma(t\rightarrow 0)=2$ and at long times $\Gamma(t)\rightarrow 1$. This equation indicates that calculations with nonzero ΔR are expected to *underestimate* the true $P_s(t)$.

B. Fourier expansion of diffusion eigenfunctions

In the Fourier method, the eigenstates are found by solving a matrix eigenvalue problem for the Fourier expansion coefficients $\tilde{u}_{n\mathbf{q}}(\mathbf{G})$, obtained from the differential equation (2.10) by using expansions such as Eq. (2.13). The transformation to a matrix eigenvalue problem is complicated by the fact that the boundary condition (2.11) must also be imposed. For the nonabsorbing case ($\rho=0$), this was done by extending Eq. (2.10) to the *entire volume* V of pore space plus matrix space in such a way that Eq. (2.11) is automatically satisfied [22,23]. The resulting matrix eigenvalue problem was then solved by standard numerical methods. For a system comprised of a simple cubic array of spherical obstacles, we included reciprocal lattice vectors $\mathbf{G}=(2\pi/a)(n_x,n_y,n_z)$ with integer components n_x,n_y,n_z ranging from -4 to 4. This translates to a matrix of size 729×729. Using this approach, it was possible to treat small, nonoverlapping obstacles, as well as large, overlapping ones. To evaluate the RTOP, the $\mathbf{q}$ sum in Eq. (2.16) was accomplished by solving Eqs. (2.10)–(2.12) for 512 different $\mathbf{q}$ values uniformly distributed over the first Brillouin zone in reciprocal space.

When there is some absorption at the pore-matrix interface, the eigenstates were found by expanding them in a series of $\rho=0$ eigenstates. The eigenvalue problem of Eqs. (2.10)–(2.12) is thereby translated into a matrix eigenvalue problem where the eigenvectors are the required expansion coefficients [24]. Again, this was solved using standard numerical methods.

To conclude this discussion we note that numerical simulation and eigenvalue techniques are complementary in their treatment of the RTOP. From Eq. (2.16) it is clear that the eigenvalue expansion will converge rapidly at long times. However, at short times the results will be considerably less reliable because the higher eigenvalue bands (i.e., $\lambda_{n\mathbf{q}}$ with large values of the band index n) cannot be calculated very accurately. By contrast, in the simulations the short time behavior is relatively easy to calculate [9], while at long times it becomes increasingly difficult to obtain good statistics, and this limits the accuracy of the subsequent $P(t)$ estimates.

C. PGSE experiments

We have applied the PGSE technique to measure $P_s(t|\rho)$ in two samples comprised of unconsolidated ran-

domly packed spherical beads, saturated with distilled water. The diameter of the beads, $2R_0$, was in the range $380 \leqslant 2R_0 \leqslant 515$ μm in the first sample and $47 \leqslant 2R_0 \leqslant 57$ μm in the second sample. The measurements were performed with a GE 2.0 T CSI-II imaging spectrometer operating at 85.56 MHz for protons and equipped with self-shielding gradient coils capable of delivering a maximum gradient strength of 20 G/cm. The measurements on the smaller beads were performed using self-shielding gradient coils capable of delivering a maximum gradient strength of 280 G/cm. The temperature of the sample was controlled at 25.0 °C.

We determined independently the ratio S/V_p for each sample by an analysis of the short time behavior of the diffusion coefficient $D(t)$ [6,10]. The measured values were $(48.4\mu\text{m})^{-1}$ and $(5.3\mu\text{m})^{-1}$, respectively. This is consistent with the bead diameters stated above. For monosized sphere packs, the ratio S/V_p is related to the bead diameter by $S/V_p = 6(1-\phi)/(2R_0\phi)$. Assuming a random packing porosity of $\phi = 0.38$, we obtain $S/V_p \approx (45.7\mu\text{m})^{-1}$ and $(5.3\mu\text{m})^{-1}$, respectively. For each sample, we have measured $M(\mathbf{k},t)$ as a function of $\mathbf{k}$ for three diffusion times t. The times were 250 ms, 1 s, and 2 s for the large beads, and 160 ms, 500 ms, and 1.5 s for the small beads. The NMR pulse sequence used is based on the stimulated spin echo. Each gradient pulse is divided into a pair of half-sine-shaped bipolar pulses, separated by a π pulse. This attenuates any effects due to background gradients. A detailed description of this pulse sequence was given by Latour *et al.* [30]. The duration of each half-sine-shaped pulse was $\delta = 1.5$ ms. The wave vector $\mathbf{k}$ was changed by increasing the gradient strength g while keeping δ fixed. In our measurements, g was stepped up in equal intervals up to some value $g_{\max}$. The maximum gradient strength $g_{\max}$ was adjusted for each sample and diffusion time by requiring that the signal decayed to about 3×10^{-4} of its initial value and became comparable to the noise level. We measured separately the linearity of the spectrometer and corrected for any deviations. The measured echo amplitudes were normalized with respect to the extrapolated amplitude $M(t) \equiv \lim_{k\to 0} M(k,t)$, as described in [20]. This corresponds to a normalization with respect to the number of surviving walkers after time t.

If the medium being studied is isotropic, Eq. (2.6) reduces to a radial integration

$$P(t|\rho) = \frac{4\pi}{(2\pi)^3}\int_0^\infty M(k,t)k^2 dk. \tag{3.6}$$

In order to apply this equation to our data, we have to deal with three complications already mentioned above: The measurements only cover a finite range in k space, the gradient pulse width δ is finite, and there is surface relaxation.

Let us first discuss the effect of limited coverage in k space. In Fig. 1, we present the quantity

$$\mathcal{P}_s(k_{\max},t) \equiv \frac{(4\pi D_0 t)^{3/2} 4\pi}{(2\pi)^3}\int_0^{k_{\max}} \frac{M(k,t)}{M(t)} k^2 dk \tag{3.7}$$

as a function of $k_{\max}$. In the limit $k_{\max}\to\infty$, $\mathcal{P}_s(k_{\max},t)$ goes over to $P_s(t|\rho)$. Inspection of Fig. 1 shows clearly that for the largest experimentally accessible wave vectors, the integral in Eq. (3.7) has not yet fully reached its asymptotic value. The limitations on the wave vector set the smallest distance, $l_{\min}$, that can be probed by PGSE techniques, typically $l_{\min} \sim 1/k_{\max}$. In general, there might be structural features on a length scale smaller than $l_{\min}$ and the quantity $P_s(t|\rho)$ cannot be extracted. However, for the largest gradients used, $l_{\min} \sim 1/k_{\max}$ is smaller than all the length scales characterizing the pore geometry in our samples, and we may use the asymptotic behavior of $M(k,t)$ for large values of k [11],

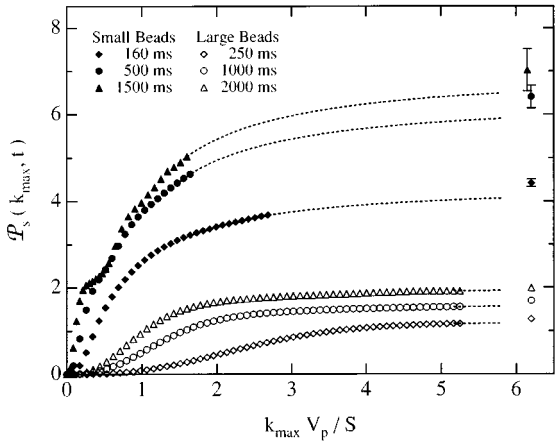

FIG. 1. Normalized integral of the measured echo amplitude $M(k,t)$ vs upper limit of integration $k_{\max}$ for two different samples and three diffusion times for each sample. The dashed lines indicate the extrapolation of the integral as discussed in the text. The extrapolated values for $k_{\max}\to\infty$ are indicated on the right with error bars.

$$M(k,t)|_{k\to\infty} = \frac{S}{V_p}\frac{2\pi}{k^4}\langle G(\mathbf{r},\mathbf{r},t)\rangle_{\mathbf{r}\in\Sigma} \sim \frac{1}{k^4}, \tag{3.8}$$

where $\langle G(\mathbf{r},\mathbf{r},t)\rangle_{\mathbf{r}\in\Sigma}$ is the probability of return to the origin for spins initially on the pore-grain interface Σ. Our measurements show that $M(k,t)$ has reached this k^{-4} behavior at the largest k values in all cases and that Eq. (3.8) can be used to extrapolate $M(k,t)$. In Fig. 1 this extrapolation is represented by the dashed lines, while the values of the extracted $P_s(t|\rho)$ are shown on the right along with their estimated uncertainties.

The correction for finite gradient pulse width δ has been considered by Mitra and Halperin [31]. They showed that for square shaped pulses of width δ, the measured values for $P_s(t|\rho)$ are too high by a factor of $(1+0.3S/V_p\sqrt{D_0\delta})$. They have not analyzed the exact pulse sequence used in our experiments, but we can use this expression as a first order estimation of the corrections. If we use an effective pulse width of $4\delta/\pi$ for our two half-sine-shaped pulses, we get a correction of 1.01 for the large beads, and 1.12 for the small beads, respectively. We have included these corrections in the data shown below.

In a separate experiment, we determined the surface relaxivity ρ for the two samples and obtained $\rho < 10^{-6}$ m/s for the small copolymer spheres and $\rho = 10^{-5}$ m/s for the large glass beads. The dimensionless parameter characterizing surface relaxation, $\rho V_p/SD_0$, is then $< 2\times10^{-3}$ and 0.21, respectively. These values indicate that surface relaxation will

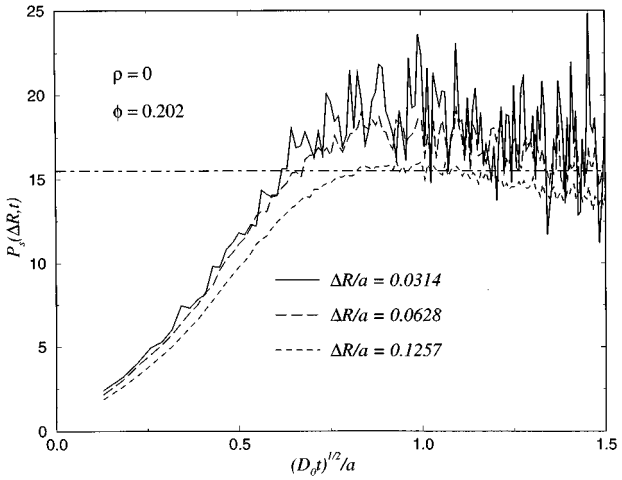

FIG. 2. For the consolidated simple cubic sphere pack, simulation data for the normalized RTOP are shown for three values of $\Delta R/a$. (Here a is the edge length of the cubic unit cell.) The horizontal (dot-dashed) line represents the asymptotic limit of Eq. (2.19).

only affect the measurements of the large beads. The effect of finite ρ on the short time behavior of $P_s(t|\rho)$ has been studied in [9] with computer simulations, where it was shown that finite ρ decreases the measured values of $P_s(t|\rho)$ in quantitative agreement with the experiments.

IV. RESULTS

In Figs. 2 and 3 we present numerical simulation data for the normalized RTOP $P_s(\Delta R,t)$ for the consolidated simple cubic and dense random packings. In both sets of calculations we tracked the motion of roughly 10^6 walkers and the data presented correspond to a sum over the first 4, 8, and 16 bins at each time, t. The noisy character of these data reflects the fact that, at long times, the probability that a given walker will remain close to its launch site is very small. In

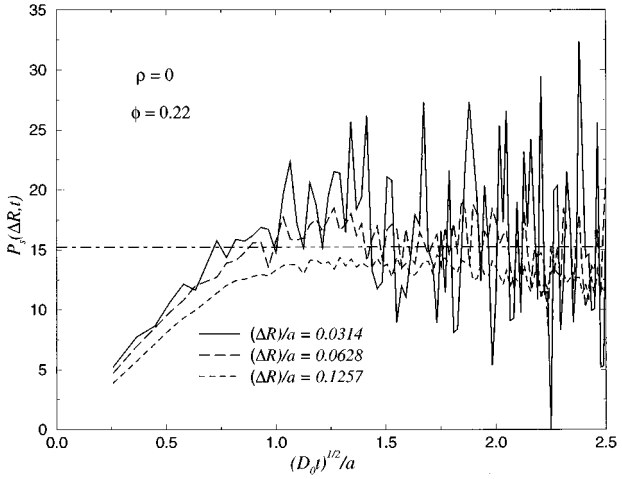

FIG. 3. For the consolidated random sphere pack, simulation data for the normalized RTOP are shown for three values of $\Delta R/a$. (Here $a=2R_0$, where R_0 is the mean sphere diameter.) The horizontal (dot-dashed) line represents the asymptotic limit of Eq. (2.19).

both figures it is clear that, as the value of ΔR decreases, the $P_s(\Delta R,t)$ values increase as suggested by Eq. (3.4). Also evident is the expected trend toward increased levels of noise as ΔR decreases. Even with these statistical limitations, there is clear evidence in the data presented in Fig. 2 to suggest that the approach to the limit of Eq. (2.19) is *not* simply monotonic. By contrast, in all $[\rho=0]$ examples studied to date, $D(t)$ decreases monotonically between its short and long time limiting values.

Clearly, it is of interest to develop a systematic approach to the smoothing of the kind of raw data shown in Figs. 2 and 3. This is especially true in light of the large number of random walkers already used; devoting more CPU time to performing even more simulations would lead to only a very small improvement in the quality of the data. Instead of that, we adopted a smoothing technique based on singular value decomposition (SVD) [32]. This is a matrix decomposition technique, applicable to arbitrary rectangular matrices, analogous to the eigenvalue decomposition of Hermitian matrices. Given the raw simulation data, $P(R_m,t_n)$, we form the covariance matrices

$$A_{m,m'}=\sum_{n=1}^{N_t} P(R_m,t_n)P(R_{m'},t_n), \tag{4.1}$$

$$B_{n,n'}=\sum_{m=1}^{N_R} P(R_m,t_n)P(R_m,t_{n'}), \tag{4.2}$$

where N_t and N_R are the number of elements in the temporal and spatial arrays. If we denote the set of eigenvectors of $A_{m,m'}$ as $\{\alpha_k(R_m)\}$, and the eigenvectors of $B_{n,n'}$ as $\{\beta_k(t_n)\}$, the SVD of $P(R_m,t_n)$ is

$$P(R_m,t_n)=\sum_{k=1}^{N} \lambda_k\alpha_k(R_m)\beta_k(t_n), \tag{4.3}$$

where $N=\min\{N_t,N_R\}$. Typically, we found that there were only two or three dominant eigenvalues (or singular values) λ_k, so that the above summation can be truncated by including just these modes. The appearance of a few large singular values indicates that the data can be approximated by a low rank space-time matrix $P(R_m,t_n)$. Discarding the smaller singular values corresponds to removing noise uncorrelated in space and time, and therefore achieves a smoothing of the original data.

In Figs. 4 and 5 we show the smoothed versions of the simulation data originally presented in Figs. 2 and 3. In both figures the curves correspond to $\Delta R=4\,\delta R$ and, in addition to being smoothed, the curves have been adjusted to represent the $\Delta R\to 0$ limit by the application of Eq. (3.4). [Here we have taken $\Gamma(t)=1$, the value appropriate for long times [21,9].] Shown also in these figures are the two straight line asymptotes derived from Eqs. (1.3) and (2.19). [The values of $D_{\rm eff}$ were taken from the eigenvalue calculation for Fig. 4 and from long time diffusion simulations for Fig. 5.] In Fig. 4 the smoothed simulation data are compared to the results of the eigenvalue expansion [33]. The agreement between these two calculations is now quite satisfactory. The most interesting feature in these figures is the clearly defined maximum in the normalized RTOP. In this connection, note

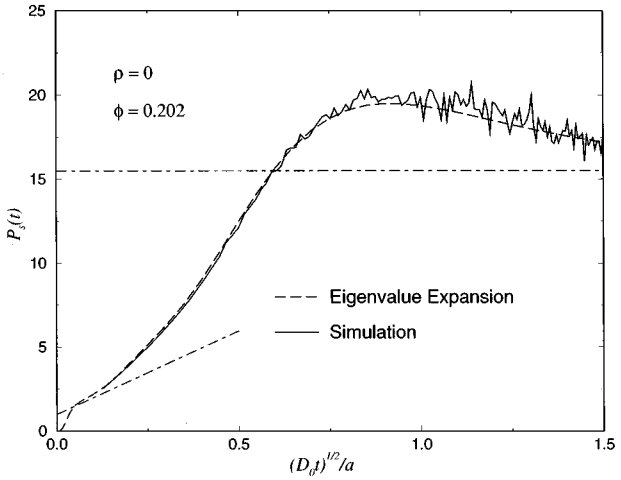

FIG. 4. For the consolidated simple cubic packing, eigenvalue expansion results for the normalized RTOP are compared to smoothed data based on SVD analysis of the corresponding numerical simulations. The simulation data have been adjusted to the $\Delta R \to 0$ limit using Eq. (3.4). The two dot-dashed lines represent the asymptotic limits of Eqs. (1.3) and (2.19).

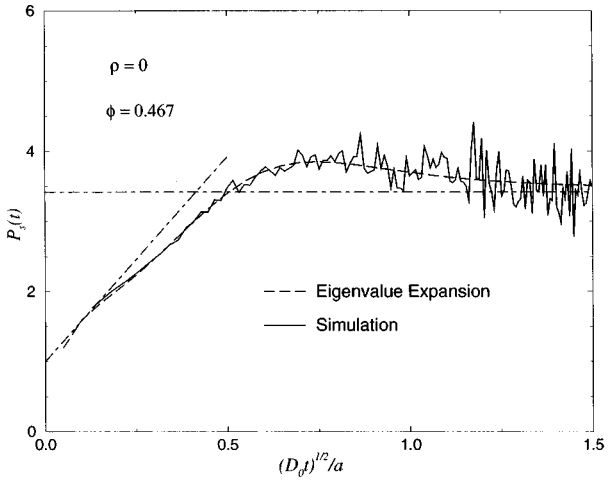

FIG. 6. For the unconsolidated simple cubic packing, eigenvalue expansion results for the normalized RTOP are compared to smoothed data based on SVD analysis of the corresponding numerical simulations. The simulation data have been adjusted to the $\Delta R \to 0$ limit using Eq. (3.4). The two dot-dashed lines represent the asymptotic limits of Eqs. (1.3) and (2.19).

that the $t=\infty$ value (i.e., the horizontal straight line asymptote) shown in these figures is quite accurate, therefore, even though the maximum in $P_s(t)$ is not manifest in the simulation results plotted in Fig. 5, nevertheless the conclusion that there is a maximum is very reliable. Both $P(t)$ and $P_0(t)$ decrease monotonically as t increases. That their ratio shows a maximum implies that, at intermediate times, the rate at which $P(t)$ decreases is *reduced* by the blocking effect of the grains. [Indeed, in the special case of isolated pores, $P(t)$ does not vanish as $t \to \infty$, and $P_s(t)$ *diverges*.] At very long times, diffusing particles will move successfully between neighboring pores; at intermediate times, however, there is a *bounce back* effect when the particles first reflect off the walls. This bounce back effect serves to enhance the RTOP and is responsible for the maximum in Figs. 4 and 5. The location of this maximum defines a new effective pore size parameter whose value is not expected to be greatly influenced by the interfacial surface area. In this sense, this new parameter is analogous to the location of the quasidiffraction peaks seen in the $M(\mathbf{k},t)$ curves, which also first appear at intermediate times [17,6]. We note that the maximum in Fig. 4 is considerably more pronounced than that in Fig. 5. In disordered systems the existence of the maximum is controlled by two competing effects. To some extent, the *bounce back* effect will be suppressed by random fluctuations in the pore sizes; on the other hand, in disordered systems diffusing particles may be effectively trapped in very small pores and thus make a very large contribution to the RTOP.

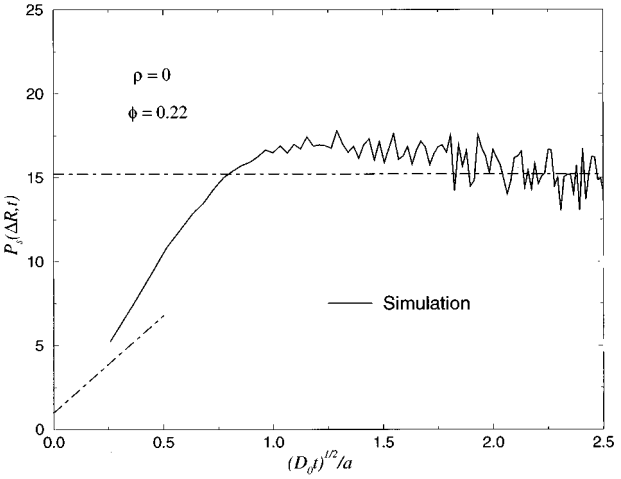

FIG. 5. For the consolidated dense random sphere pack, simulation results for the normalized RTOP are shown after SVD smoothing. The simulation data have been adjusted to the $\Delta R \to 0$ limit using Eq. (3.4). The two dot-dashed lines represent the asymptotic limits of Eqs. (1.3) and (2.19).

In Figs. 6 and 7 we show the smoothed simulation data corresponding to $\Delta R = 4\,\delta R$ for the unconsolidated simple cubic and dense random packings. [As in Figs. 4 and 5 the curves have been adjusted to represent the limit $\Delta R \to 0$.] In Fig. 6 the simulations are compared to the eigenvalue expansion while in Fig. 7 the simulation data are compared to the measurements discussed in Sec. III C. In Fig. 6 the maximum in the normalized probability is again evident but is now much less pronounced. On physical grounds this is to be expected because at higher porosities, diffusing particles can move more easily into neighboring pores and the *bounce back* effect is diminished. Turning to Fig. 7, we see that the overall comparison between theory and experiment is quite reasonable and that both the measurements and the simulations lie above the long time asymptote. Together with the data presented in Fig. 5, these results suggest that the behavoir of $P(t)$ in disordered systems may be qualitatively similar to that found in periodic models. We intend to explore this issue further with additional experimental and numerical work.

The calculations described above were all carried out with $\rho = 0$. Intuitively, we expect that interfacial relaxation will *strengthen* the maximum observed in $P_s(t)$. With nonzero

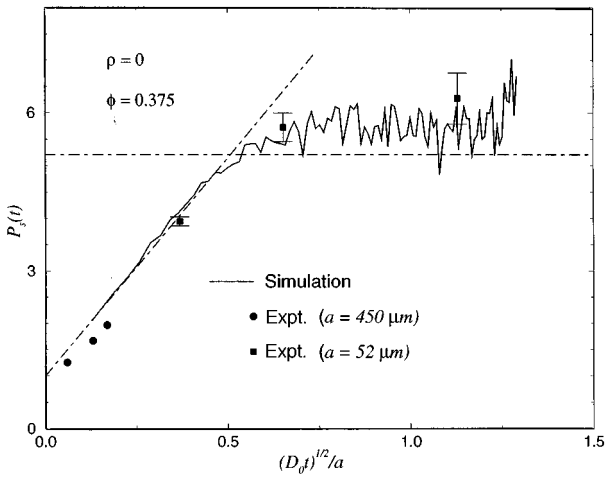

FIG. 7. For the unconsolidated dense random sphere pack, simulation results for the normalized RTOP are compared with experimental data. The simulation data have been adjusted to the $\Delta R \to 0$ limit using Eq. (3.4). The two dot-dashed lines represent the asymptotic limits of Eqs. (1.3) and (2.19). The six experimental points discussed in connection with Fig. 1 are also shown. Note that, for the large beads used in some of the measurements, ρ is not entirely negligible. Nevertheless, its rather small value (i.e., $\rho V_p/SD_0 = 0.21$), plus the fact that those measurements correspond only to the short time asymptotic regime, mean that the results should not differ very much from the ideal $\rho = 0$ case.

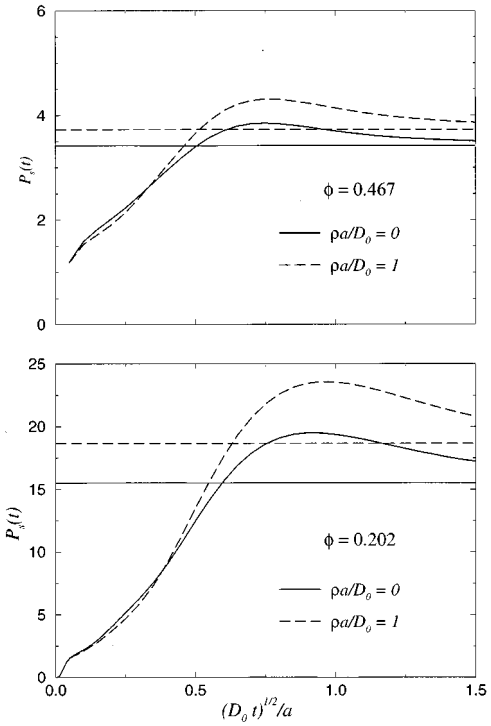

FIG. 8. The effects of surface relaxation on the RTOP are illustrated for the touching sphere (upper panel) and overlapping sphere (lower panel) simple cubic packings. Note that, to leading order, the short time behavior of $P_s(t)$ is *not* affected by ρ [9].

ρ, the particles most likely to survive are those that do not move very far from their point of origin and therefore do not interact strongly with the pore-grain interface. Thus, in Fig. 8 we see that, for the periodic sphere packs discussed above, eigenvalue calculations indeed indicate that the maximum in $P_s(t)$ is enhanced in the $\rho a/D_0 = 1$ case. We expect that random walk simulations would exhibit the same effects; they would, however, be considerably more involved than the corresponding eigenvalue calculations [11,28]. Here too, the values of $P_s(\infty)$ are shown as horizontal straight lines—they were calculated from the low lying diffusion eigenstates [see Eq. (2.19)].

As we noted above, the calculations presented here are not intended to describe the *short time* behavior of $P_s(t)$ with great accuracy. Nevertheless, it is of interest to examine the trends seen in Figs. 4–7. For the two low porosity systems (Figs. 4 and 5) the calculated results clearly curve upward from their short time asymptotes. For $\phi = 0.38$ (Fig. 7) the calculations remain essentially in line with the short time asymptote up to surprisingly long times. Finally, at the highest porosity (Fig. 6), the calculated curve has crossed over and now lies below the short time asymptote. This behavior is, of course, consistent with the appearance of a more pronounced maximum at intermediate times in the lower porosity systems.

V. CONCLUSIONS

We have studied the intermediate and long time behavior of the normalized RTOP, $P_s(t)$. Like the time dependent diffusion coefficient $D(t)$, this function is controlled by the pore surface area at short times and by the effective electrical conductivity or formation factor F at long times. However, this function exhibits considerably more varied and interesting behavior than $D(t)$. We believe that $P_s(t)$, as well as $P_s(t|\rho)$ for $\rho \neq 0$, will be important indicators of the structure of the underlying porous media. Our principal findings are as follows:

(a) In ordered (periodic) porous media $P_s(t)$ can be calculated by either eigenvalue expansions or numerical simulations. The two methods are in excellent agreement. (b) In ordered (periodic) porous media $P_s(t)$ crosses above its long time asymptote and exhibits a well defined maximum at intermediate times. This behavior is predicted by a theorem that constrains the behavior of the lowest band of eigenvalues. Physically, this maximum is associated with the *reflection* of diffusing particles from the pore grain interface. (c) In the random systems studied here, numerical simulations again suggest that $P_s(t)$ will exhibit a maximum at intermediate times. In unconsolidated dense random sphere packs, the simulation data and PGSE measurements are generally in good agreement. (d) Systematic trends are evident in the manner at which $P_s(t)$ moves away from its asymptotic limit at short times. This behavior is again related to the degree of hindrance to diffusion caused by the solid matrix.

ACKNOWLEDGMENTS

We would like to acknowledge useful conversations with B. I. Halperin and D. L. Johnson. M.D.H. acknowledges experimental assistance by K. G. Helmer and C. H. Sotak. D.J.B. was supported, in part, by grants from the U.S.-Israel Binational Science Foundation and the Israel Science Foundation.

[1] M. Kac, Am. Math. Monthly **73**, 1 (1966).
[2] P. G. de Gennes, C. R. Acad. Sci. **295**, 1061 (1982).
[3] R. Jensen, Nature **355**, 591 (1992).
[4] C. Gordon, D. Webb, and S. Wolpert, Bull. Am. Math. Soc. **27**, 134 (1992).
[5] S. Sridhar and A. Kudrolli, Phys. Rev. Lett. **72**, 2175 (1994).
[6] P. P. Mitra, P. N. Sen, L. M. Schwartz, and P. Le Doussal, Phys. Rev. Lett. **68**, 3555 (1992).
[7] P. P. Mitra, P. N. Sen, and L. M. Schwartz, Phys. Rev. B **47**, 8565 (1993).
[8] P. P. Mitra, L. L. Latour, R. L. Kleinberg, and C. H. Sotak, J. Magn. Reson. A **114**, 47 (1995).
[9] M. D. Hürlimann, L. M. Schwartz, and P. N. Sen, Phys. Rev. B **51**, 14 936 (1995).
[10] L. L. Latour, P. P. Mitra, R. L. Kleinberg, and C. H. Sotak, J. Magn. Reson. A **101**, 342 (1993).
[11] P. N. Sen, L. M. Schwartz, P. P. Mitra, and B. I. Halperin, Phys. Rev. B **49**, 215 (1994).
[12] D. J. Bergman, following paper, Phys. Rev. E **55**, 4235 (1997).
[13] E. O. Stejskal and J. E. Tanner, J. Chem. Phys. **42**, 288 (1965).
[14] E. O. Stejskal, J. Chem. Phys. **43**, 3597 (1965).
[15] J. E. Tanner, J. Chem. Phys. **52**, 2523 (1970).
[16] P. T. Callaghan, *Principles of Nuclear Magnetic Resonance Microscopy* (Oxford University Press, Oxford, 1991); this book describes most of the relevant experimental and theoretical research in the field of NMR in porous media that was done before 1990, including references.
[17] P. T. Callaghan, A. Coy, D. MacGowan, K. J. Packer, and F. O. Zelaya, Nature **351**, 467 (1991).
[18] P.T. Callaghan, D. MacGowan, K. J. Packer, and F. O. Zelaya, Mag. Res. Imaging **9**, 663 (1991).
[19] P. T. Callaghan, A. Coy, T. P. J. Halpin, D. MacGowan, K. J. Packer, and F. O. Zelaya, J. Chem. Phys. **97**, 651 (1992).
[20] M. D. Hürlimann, K. G. Helmer, L. L. Latour, and C. H. Sotak, J. Magn. Reson. A **111**, 169 (1994).
[21] P. N. Sen, M. D. Hürlimann, and T. M. de Swiet, Phys. Rev. B **51**, 601 (1995).
[22] D. J. Bergman and K. J. Dunn, Phys. Rev. B **50**, 9153 (1994).
[23] K. J. Dunn and D. J. Bergman, J. Chem. Phys. **102**, 3041 (1995).
[24] D. J. Bergman and K. J. Dunn, Phys. Rev. E **51**, 3401 (1995).
[25] D. J. Bergman, Phys. Rep. **43**, 377 (1978).
[26] D. J. Bergman, in *Les Mèthodes de l'Homogénéisation: Théorie et Applications en Physique*, Préface by R. Dautray (Editions Eyrolles, Paris, 1985), pp. 1–128.
[27] J. R. Banavar and L. M. Schwartz, in *Molecular Dynamics in Restricted Geometries*, edited by J. Klafter and J. M. Drake (Wiley, New York, 1989), p. 273.
[28] D. J. Bergman, K. J. Dunn, L. M. Schwartz, and P. P. Mitra, Phys. Rev. E **51**, 3393 (1995).
[29] J. N. Roberts and L. M. Schwartz, Phys. Rev. B **31**, 5190 (1985); L. M. Schwartz and S. Kimminau, Geophysics **52**, 1402 (1987).
[30] L. L. Latour, L. Li, and C. H. Sotak, J. Magn. Reson. B **101**, 72 (1993).
[31] P. P. Mitra and B. I. Halperin, J. Magn. Reson. A **113**, 94 (1995).
[32] W. H. Press, B. P. Flannery, S. A. Teulolsky, and W. T. Vetterling, *Numerical Recipes, The Art of Scientific Computing (Fortran Version)* (Cambridge University Press, Cambridge, 1990), Secs. 2.9 and 14.5.
[33] In order to connect between the time scales of the two computational methods we use the identity $D_0 t/a^2 = N\epsilon^2/(6a^2)$, where N is the number of random walk time steps. Thus, with $\epsilon/a = 0.01$, we have $t = 10^{-4} N a^2/(6D_0)$.